JMEPEG (2011) 20:289–297
DOI: 10.1007/s11665-010-9666-5

1059-9495/$19.00

Study of Steel Emissivity Characteristics and Application of Multispectral Radiation Thermometry (MRT)

Chang-Da Wen

(Submitted July 13, 2009; in revised form February 22, 2010)

Experiments were first conducted to measure the emissivity values of a variety of steel samples at 700, 800, and 900 K. The effects of wavelength, temperature, alloy composition, and heating time on emissivity were investigated. Multispectral radiation thermometry (MRT) with linear emissivity models (LEMs) and log-linear emissivity models (LLEs) were then applied to predict surface temperature. Parametric influences of the number of wavelengths and order of emissivity models were examined. Results show that the spectral emissivity decreases with increasing wavelength and increases with increasing temperature. Steel with higher chromium content has lower emissivity value because of the chromium oxide protection layer. The spectral emissivity reaches steady state after the third hour heating due to the surface oxidation becoming fully developed. Increasing the order of polynomial and increasing the number of wavelengths cannot improve temperature measurement accuracy. Overall, the first-order LEM and the first-order LLE showed the best accuracy for different alloys, the number of wavelengths, and temperatures.

Keywords emissivity, multispectral radiation thermometry, steel, temperature measurement

1. Introduction

Steel is undeniably the most important metallic material in the world. With its inherent features of strength, hardness, ease of fabrication, fire and heat resistance, impact resistance, and corrosion resistance, it has been used extensively in many applications, from small metallic parts to large structural members.

With increased competitiveness and the requirements for higher product quality and lower cost, there is an urgent need for the steel industry to develop more efficient and effective techniques to produce better products with less waste. A key issue to achieve higher performance in manufacturing process is to accurately measure the metal surface temperature.

Most processes in steel production, such as forging, extrusion, and rolling are highly temperature dependent, and accurate temperature measurement achieves better metallurgical quality, improves product reliability and reproducibility, and reduces production cost.

Thermocouple or other types of contact thermometers are very commonly used to measure the surface temperature in most industries. However, contact methods are undesirable in some processes because of the impracticability in moving material situations, and the physical and chemical changes of the surface. On the other hand, the contact method currently in use may not be accurate enough to meet the industry requirement. As a result, there is a need for a more accurate, nondestructive, and more simple approach. One such approach is a non-contact radiometric method.

Chang-Da Wen, Department of Mechanical Engineering, National Cheng Kung University, No. 1, University Road, Tainan 701, Taiwan. Contact e-mail: alexwen@mail.ncku.edu.tw.

2. Radiation Thermometry

Radiation thermometry, a non-contact temperature measurement method, utilizes spectral intensity measured from the target surface to infer the true temperature. Radiometric system generally can be divided into three parts: the target, the environment, and the radiation thermometer itself. The exitent spectral intensity, $L_{\lambda,\text{meas}}$, measured by the radiation thermometer can be comprised of four components,

$$L_{\lambda,\text{meas}}(\lambda, T) = L_{\lambda,\text{e}}(\lambda, T) + L_{\lambda,\text{ref}} + L_{\text{e}} + L_{\text{s}}, \quad \text{(Eq 1)}$$

where $L_{\lambda,\text{e}}$ is the self-emitted intensity from the target, $L_{\lambda,\text{ref}}$ is from the surrounding irradiation reflected by the target surface, L_{e} is due to the target irradiation reflected by the surrounding and then target itself, and L_{s} is from the atmospheric scattering and absorption (H_2O, CO_2, dust particles, etc.). If the radiation between the target and surrounding is between a small surface and a large enclosure, L_{e} can be neglected due to the blackbody assumption of the surrounding. In the absence of atmospheric line-of-sight absorption or emission, then L_{s} can also be negligible. From the law of energy conservation and the application of Kirchhoff's law, for an opaque material the reflectivity can be determined as

$$\rho_\lambda = 1 - \varepsilon_\lambda. \quad \text{(Eq 2)}$$

Therefore, the exitent spectral intensity, $L_{\lambda,\text{meas}}$, of an opaque real surface is then comprised of only the emitted component $L_{\lambda,\text{e}}$, and the reflected component $L_{\lambda,\text{ref}}$, and can be simplified as

$$L_{\lambda,\text{meas}}(\lambda, T) = \varepsilon_\lambda L_{\lambda,\text{b}}(\lambda, T) + (1 - \varepsilon_\lambda) L_{\lambda,\text{b}}(\lambda, T_{\text{sur}}), \quad \text{(Eq 3)}$$

where both $L_{\lambda,\text{b}}(\lambda,T)$ and $L_{\lambda,\text{b}}(\lambda,T_{\text{sur}})$ can be calculated from the Planck distribution. With known ε_λ, the target surface

Nomenclature	
a_0	first unknown coefficient of emissivity model
a_1	second unknown coefficient of emissivity model
a_n	$(n + 1)$th unknown coefficient of emissivity model
c_1	first thermal radiation constant
c_2	second thermal radiation constant
DWRT	dual-wavelength radiation thermometry
L_e	spectral intensity of target surface emission reflected back by surroundings
L_s	spectral intensity of radiation associated with scattering and absorption
$L_{\lambda,b}$	spectral intensity of blackbody radiation
$L_{\lambda,e}$	spectral intensity of radiation emitted by target surface
$L_{\lambda,gen}$	generated spectral intensity of radiation
$L_{\lambda,meas}$	measured spectral radiation intensity
$L_{\lambda,ref}$	spectral intensity of irradiation from surroundings that is reflected by target surface
LEM	linear emissivity model
LLE	log-linear emissivity model
MRT	multispectral radiation thermometry
n	required minimum number of wavelengths
N	total number of wavelengths available in the examined wavelength range
SRT	spectral radiation thermometry
T	surface temperature
T_{sur}	temperature of surroundings
Greek Symbols	
ε_λ	spectral emissivity
λ	wavelength
ρ_λ	spectral reflectivity
χ^2	least-squares error
Subscripts	
b	blackbody
e	emitted
gen	generated
meas	measured
ref	reflected
s	scatter
sur	surroundings
λ	spectral

temperature T can be determined using the Eq 3 from the measured spectral intensity, $L_{\lambda,meas}$. In the same manner, emissivity can be determined by the Eq 3 from the measured spectral intensity, $L_{\lambda,meas}$, and known target surface temperature T. Emissivity measurement was conducted in this study through this method.

Determining the temperature can be accomplished by three categories of radiation thermometry which utilize intensity measurement at different number of wavelengths: spectral, dual-wavelength, and multispectral. Spectral radiation thermometry requires the intensity measurement at one wavelength and a constant emissivity value to infer the surface temperature. Dual-wavelength radiation thermometry (DWRT) utilizes the intensity measurements at two distinct wavelengths and an emissivity compensation algorithm to obtain the surface

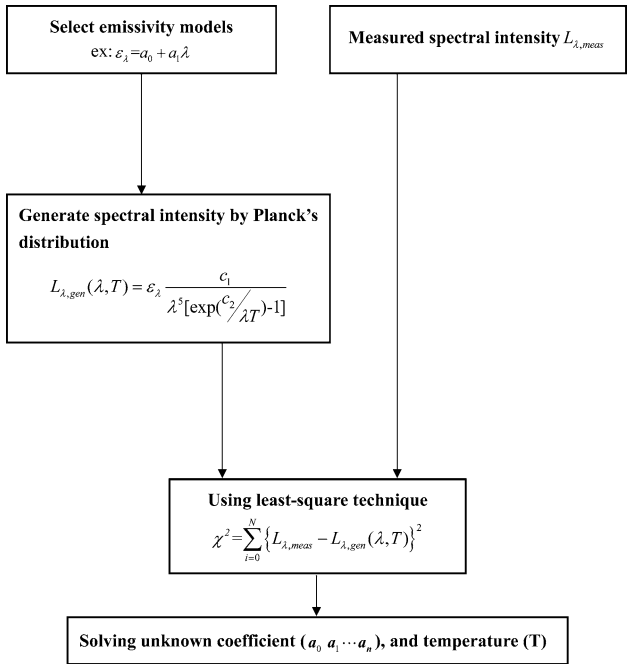

Fig. 1 MRT methodology

temperature. Multispectral radiation thermometry (MRT) employs the intensity measurements at three or more discrete wavelengths and an emissivity model to determine the surface temperature. The MRT method is preferred for its ability to enhance measurement accuracy as well as to account for the complex spectral variations of both radiation intensity and emissivity.

Two most common MRT emissivity models are examined in this study. They are log-linear emissivity model (LLE) and linear emissivity model (LEM). The least-squares technique which employs least-squares fitting of the measured intensity to simultaneously deduce the best-fit values of emissivity and temperature is used for both models. Figure 1 shows the methodology of MRT. The number of unknown coefficients in the emissivity model must be at least two less than the number of the spectral intensity values for the least-squares technique. The rationale is to determine the inferred temperature and the unknown emissivity coefficients by minimizing the chi-squared (χ^2) value of the following equation:

$$\chi^2 = \sum_{i=0}^{n} \left(L_{\lambda,\mathrm{meas},i} - L_{\lambda,\mathrm{gen},i}\right)^2, \qquad \text{(Eq 4)}$$

where $L_{\lambda,\mathrm{meas},i}$ and $L_{\lambda,\mathrm{gen},i}$ are the measured and generated values of spectral intensity, respectively. Neglecting the intensity of irradiation from the surroundings which is reflected by the target surface and applying Planck blackbody distribution, the generated spectral intensity can be simplified as

$$L_{\lambda,\mathrm{gen}}(\lambda,T) \cong \varepsilon_\lambda(\lambda) L_{\lambda,\mathrm{b}}(\lambda,T) = \varepsilon_\lambda(\lambda)\frac{c_1}{\lambda^5\left(e^{c_2/\lambda T}-1\right)}, \qquad \text{(Eq 5)}$$

where $c_1 = 1.191062 \times 10^8$ W μm^4 m^{-2} sr^{-1}, and $c_2 = 1.438786 \times 10^4$ μm K.

For emissivity models with exponential form, the linear least-squares technique can be used to determine the inferred

temperature and the unknown emissivity coefficients by minimizing the magnitude of χ^2 in the following equation:

$$\chi^2 = \sum_{i=0}^{n} \left(\ln L_{\lambda,\text{meas},i} - \ln L_{\lambda,\text{gen},i}\right)^2. \quad \text{(Eq 6)}$$

In addition, the Planck blackbody distribution, used in Eq 5 to determinate the generated value of spectral intensity, $L_{\lambda,\text{gen},i,}$ is approximated by Wien's formula,

$$L_{\lambda,\text{b}}(\lambda, T) = \frac{c_1}{\lambda^5\left(e^{c_2/\lambda T} - 1\right)} \cong \frac{c_1}{\lambda^5\left(e^{c_2/\lambda T}\right)}. \quad \text{(Eq 7)}$$

Therefore, a set of equations that is linear with respect to the temperature and the unknown emissivity coefficients can be created to simplify the computation.

For the nonlinear least-squares technique, the Planck's distribution law is used, and the iterative techniques are required to solve the equations.

The log-linear emissivity model (LLE),

$$\varepsilon_\lambda = \exp(a_0 + a_1\lambda + a_2\lambda^2 + \cdots + a_n\lambda^n), \quad \text{(Eq 8)}$$

is an exponential of an nth order polynomial in wavelength which is linear with respect to the unknown coefficients, a_i. This model has been studied by many researchers (Ref 1-7).

The linear emissivity model (LEM),

$$\varepsilon_\lambda = a_0 + a_1\lambda + a_2\lambda^2 + \cdots + a_n\lambda^n, \quad \text{(Eq 9)}$$

is an nth order polynomial in wavelength which is linear with respect to the unknown coefficients, a_i. It is empirically based and has been examined experimentally and numerically by many researchers (Ref 1, 2, 6, 8-15).

Table 1 shows the mathematical form of the LLEs and LEMs examined in this study, along with the order of polynomial function employed, and minimum number of required wavelengths incorporated in the least squares technique. For the LLE model, the linear least-squares technique, Eq 6 is used to determine the inferred temperature and the unknown emissivity coefficients, and for the LEM, Eq 4 is used.

All the radiometric methods are sensitive to changes in the spectral emissivity of the material, and they also require some knowledge of the surface emissivity. Therefore, the precise experimental measurements of the emissivity, which lead to understand the emissivity behaviors of the materials well, will be very important and helpful to develop an emissivity compensation algorithm which can accurately infer the temperature. In this study, the interdependent parametric influences of wavelength, temperature, heating time, and alloy composition on steel emissivity were first investigated experimentally.

Table 1 Mathematical function of LEMs and LLEs examined in this study

Emissivity models	Formula	Order	n (a)
Linear emissivity models (LEM)	$\varepsilon_\lambda = \exp(a_0 + a_1\lambda)$	1	4
	$\varepsilon_\lambda = \exp(a_0 + a_1\lambda + a_2\lambda^2)$	2	5
	$\varepsilon_\lambda = \exp(a_0 + a_1\lambda + a_2\lambda^2 + a_3\lambda^3)$	3	6
Log-linear emissivity models (LLE)	$\varepsilon_\lambda = a_0 + a_1\lambda$	1	4
	$\varepsilon_\lambda = a_0 + a_1\lambda + a_2\lambda^2$	2	5
	$\varepsilon_\lambda = a_0 + a_1\lambda + a_2\lambda^2 + a_3\lambda^3$	3	6

(a) n is the minimum number of wavelength required in MRT model

The most commonly used MRT emissivity compensation algorithms, LLE and LEM, were then used to examine the MRT on steel surface temperature determination.

3. Experimental Methods

The experimental apparatus, shown in Fig. 2, was primarily comprised of a spectrometer (radiation thermometer), test sample heating assembly, temperature controller, power supply, translation stage, data acquisition system, and a blackbody for calibration. Most of the apparatus was mounted atop a welded steel cart.

The sample heating assembly which includes cartridge heaters, heating copper block, test sample, and ceramic fiber blanket insulation, are shown in Fig. 3. The whole sample heating assembly was fastened by the aluminum frame and situated on a translation stage. The steel test sample was held in contact with a heating block. In order to minimize the temperature gradient, the heating block was fabricated from brass and surrounded by a thick blanket of high-temperature ceramic fiber insulation (Thermal Ceramics). Three cartridge heaters as the heat source were embedded in the heating block. A temperature controller (WATLOW) with a Chromel-Alumel (type K) thermocouple attached on the sample surface was used to heat the sample to the desired test temperature.

A Fast Infrared Array Spectrometer (FIAS) Model ES100 made by Spectraline Inc. was optically aligned in front of the test module. It was used to simultaneously measure 160 discrete spectral radiation intensity values having the wavelength range from 1.2 to 4.8 μm. The radiation intensity from the target is incident on the entrance slit, directed and split into the spectral components, and then ultimately dispersed over a staggered 160-element linear array PbSe detector. Then, the voltages and pixel numbers provided by the linear array are converted into wavelengths and intensities using pre-installed calibration curves. The data of intensity collected in each spectrum are stored at 390 Hz. The entrance port is a 6 mm-high by 0.5-mm wide slit. The FIAS accepts the incident lights at a diverging angle of ±0.25 degrees from the edges of the slit. Therefore, for example, a target placed at 120 mm in front should have the longest side of the homogeneous view area at least larger than 7.05 mm ($6 + 2 \times 120 \times \tan 0.25°$). In addition, a focusing tube may be installed to eliminate the aforementioned spatial resolution problem and an alignment HeNe laser can be installed to point the spectrometer at a desired target that is far away from the spectrometer.

In order to record and process the collected data, a computer and two ISA boards were used. The first one is a 1 MHz, 12 bit A/D board and the second one is a 32 MB memory board. The data acquisition is controlled by the drive circuit on the spectrometer. A Windows-based GUI, Infraspec Version 2, designed by Spectraline Inc. is available for basic spectrometric functions. The output can either be displayed on the Windows-based GUI or stored onto the computer memory for data analysis.

Test samples encompassing a variety of steel were supplied from the Gloria Material Technology Corporation (GMTC), and machined to the size of 40 mm × 20 mm × 5 mm. They are stainless steel (AISI 410, AISI420, and AISI 630) and tool steel (AISI H12 and AISI A6). Table 2 shows their applications, and Table 3 shows the characteristics of each major alloy constituent as percentage of weight. (wt.%) The surface profile

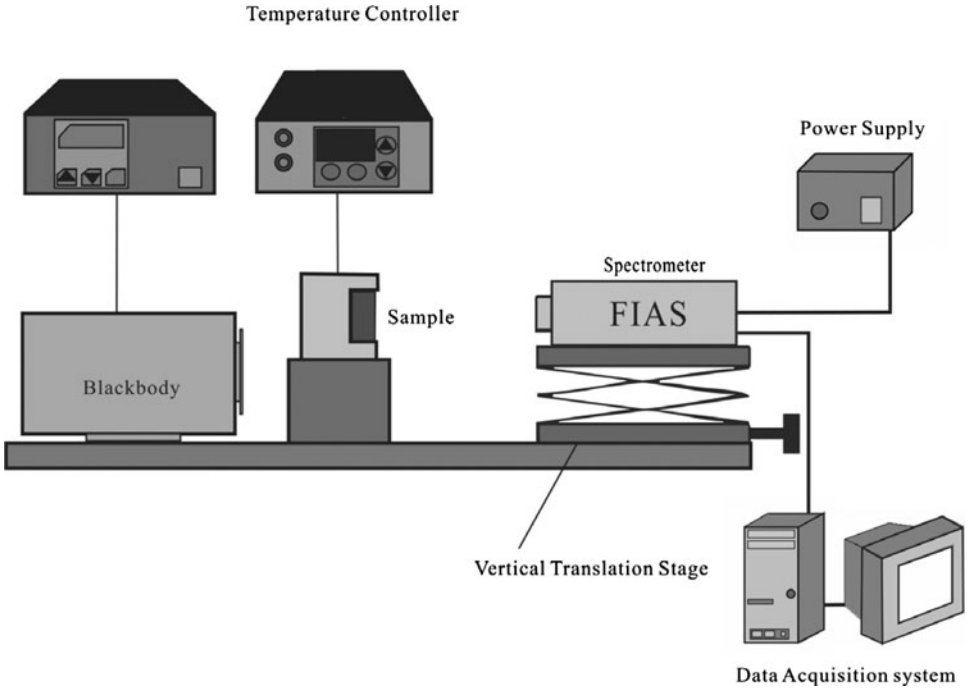

Fig. 2 Temperature measurement facility

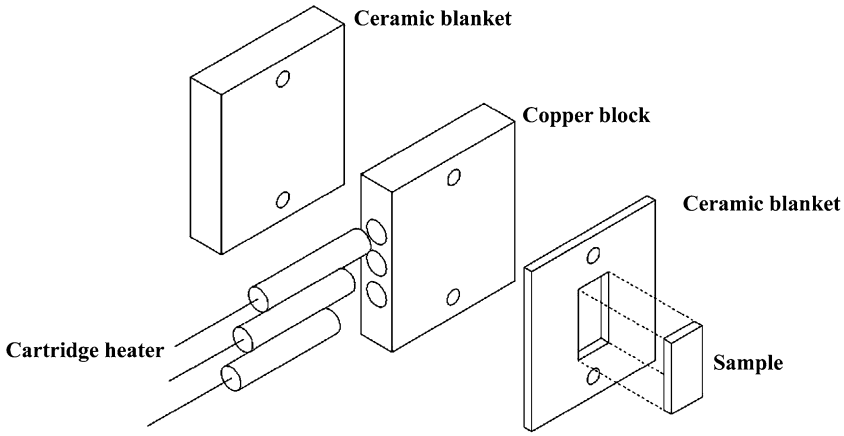

Material		Dimension (mm)	Length	Thickness	Height	Diameter
Heating assembly	Heating	Cartridge Heater	64	–	–	12.5
		Copper	80	28	90	–
		Steel	40	5	20	–
	Insulation	Ceramic fiber blanket (Front)	80	5	90	–
		Ceramic fiber blanket (Rear)	80	20	90	–

Fig. 3 Construction of steel test sample and heating assembly

and average roughness for each sample were measured by a surface profilometer (Alpha-Step MA-1450, Tencor Instrui) and shown in Fig. 4.

The test samples were first machined to the required shape and size. Before exerting any sample, the tested surface was cleaned in succession with acetone and methanol to get rid of the oils, grease, or dirt. The tested samples were handled with great care and wrapped in fine tissue to assure their surfaces were free from contact with roughening agents. The heating block was preheated to a temperature slightly above the anticipated one before heating the test sample. The test sample was then pressed against the preheated heating block to initiate heat-up. The desired sample temperature was achieved using the temperature controller to manipulate power input to the cartridge heaters. Once the temperature of the sample was stabilized, the intensity data were ready to be collected.

Table 2 Applications of steel test samples examined in this study

Type	Material	Applications
Stainless steel	AISI410	Electric appliance parts, bearing shaft (motor)
	AISI420	Plastic mold, screw
	AISI630	Car parts, medical equipment, aircraft parts
Tool steel	H12	Die (forging, casting)
	A6	Punch, measuring tool

Table 3 Constituents of steel test samples examined in this study

	Stainless steel			Tool steel	
Material	AISI410	AISI420	AISI630	H12	A6
Chemical composition, wt.%					
C	0.14	0.33	0.03	0.34	0.68
Si	0.40	0.38	0.34	0.99	0.28
Mn	0.38	0.38	0.63	0.37	2.01
Ni	0.18	0.17	4.60	0.13	0.04
Cr	12.76	12.43	15.69	5.14	1.02
Mo	0.03	0.06	0.13	1.30	0.95
Cu	0.04	0.05	3.31	0.05	0.03
P	0.018	0.022	0.021	0.021	0.017
S	0.001	0.004	0.003	0.001	0.004
V	0.02	0.03	0.08	0.28	0.01
Al	0.001	0.028	0.007	0.024	0.020
Co	0.013	0.014	0.034	0.019	0.006
W			0.03	1.10	0.01

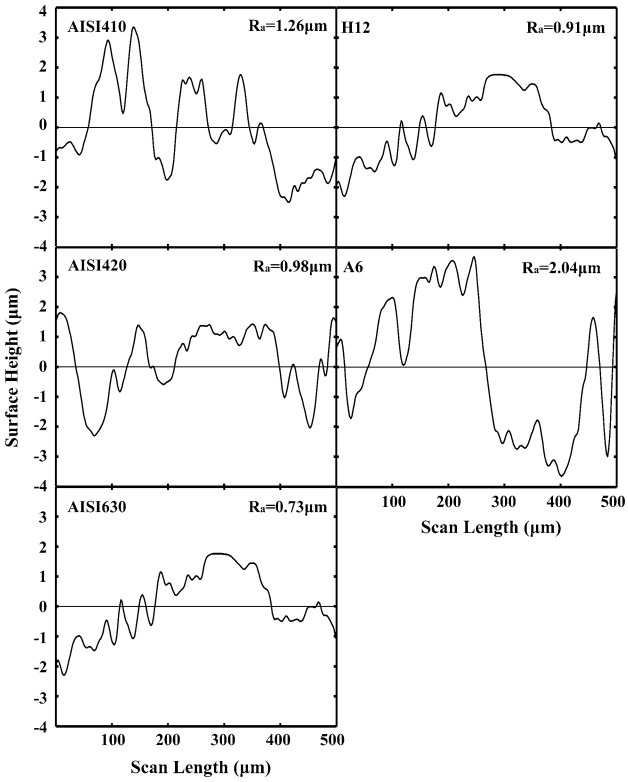

Fig. 4 Surface profiles of steel test samples

The spectrometer was first calibrated by a blackbody, RBB-1000 (MINARAD SYSTEM Inc.), and aligned with the test sample by the installed HeNe laser. The laser spot aimed at the center of the sample surface. The data of intensity in each spectrum were taken by the spectrometer and stored at 390 Hz. In this study, three temperatures, 700, 800, and 900 K were selected for measurement and analysis. All of the experiments were operated under normal laboratory conditions with a fairly constant room temperature of approximately 295 K. After the measurements were finished, the power of the heater and spectrometer was shut off. Then, the test sample was removed from the heater and cooled to room temperature.

4. Results and Discussion

Five test samples encompassing a variety of steel alloys were tested in this study. The spectral emissivity was calculated by Eq 3, where $L_{\lambda,\text{meas}}$ was measured by the spectrometer, and $L_{\lambda,b}(\lambda,T)$ and $L_{\lambda,b}(\lambda,T_{\text{sur}})$ were calculated from the Planck distribution using the sample temperature T from the temperature controller readout, and the room temperature T_{sur}, respectively. We shall now discuss of the effects of temperature, wavelength, heating time, and alloy composition on the spectral emissivity.

4.1 Effects of Wavelength

As shown in Fig. 5, the results show the emissivity distributions for AISI 410, AISI 420, AISI 630, AISI H12, and AISI A6 at 700, 800 and 900 K with wavelength ranging from 2 to 4.8 μm. The two shaded bands around 2.7 and 4.3 μm in the figure represent the atmospheric absorption and scattering bands. The former one is due to radiation caused by the room humidity and carbon dioxide, and the latter is due to the room carbon dioxide alone. According to Eq 1 and 3, the two bands should be excluded from the examined wavelength ranges since they will affect the intensity measurement and cause errors in calculating the spectral emissivity. In wavelength range shorter than 2.5 μm, the distributions are variable and the instability is due to the low signal levels and the low signal-to-noise ratios, and also the higher relative error of the calibration of FIAS in this range (Ref 16). However, in the wavelength range larger than that, all alloys exhibit the expected trend for most metallic surfaces of monotonously decreasing emissivity with increasing wavelength.

4.2 Effects of Temperature

In Fig. 5, it is apparent that the shapes of the emissivity spectra for different alloys are linear at different temperatures. Overall, with increasing temperature, the tool steel (AISI H12 and AISI A6) has drastic change in temperature than the stainless steel (AISI 410, AISI 420, and AISI 630). Moreover, the spectral emissivity value does not always increase as expected when the temperature increases. The spectral emissivity behaviors for stainless steel samples have the expected trend of most metallic surface, increasing emissivity with increasing temperature. This results from the oxidation and the change of surface color from light metallic gray into black during the heating. However, the emissivity trends for tool steel keep increasing first between 700 and 800 K, and then decreasing above 800 K. The decrease in emissivity at high temperature is attributed to the oxide layer volatility (Ref 17-19)

and the onset of melting turning the surface color from black into red.

4.3 Effects of Alloy Composition

Figure 6 shows the effect of alloying constituents on the spectral emissivity. The spectral emissivity distributions for different alloys are similar in shape, but not in magnitude. The differences in emissivity results from the variations in oxidation, which is alloy dependent. From Table 3, we observe that stainless steel contains higher weight percentages of chromium than tool steel (AISI 630 (15.69%) > AISI 410 (12.76%) > AISI 620 (12.43%) > AISI H12 (5.14%) > AISI A6 (1.02%)). The same order is also found in Fig. 6 for the magnitude of emissivity values in the opposite way. Alloys with higher chromium have lower emissivity value. For instance, the stainless steel AISI 630 containing the highest chromium content has the lowest emissivity over the whole spectral range. This is attributed to the surface chromium layer which can further prevent the alloy interior from oxidation and confine the growth of oxide layer. Therefore, for steel with high chromium, emissivity is usually lower because of the chromium oxide protection layer.

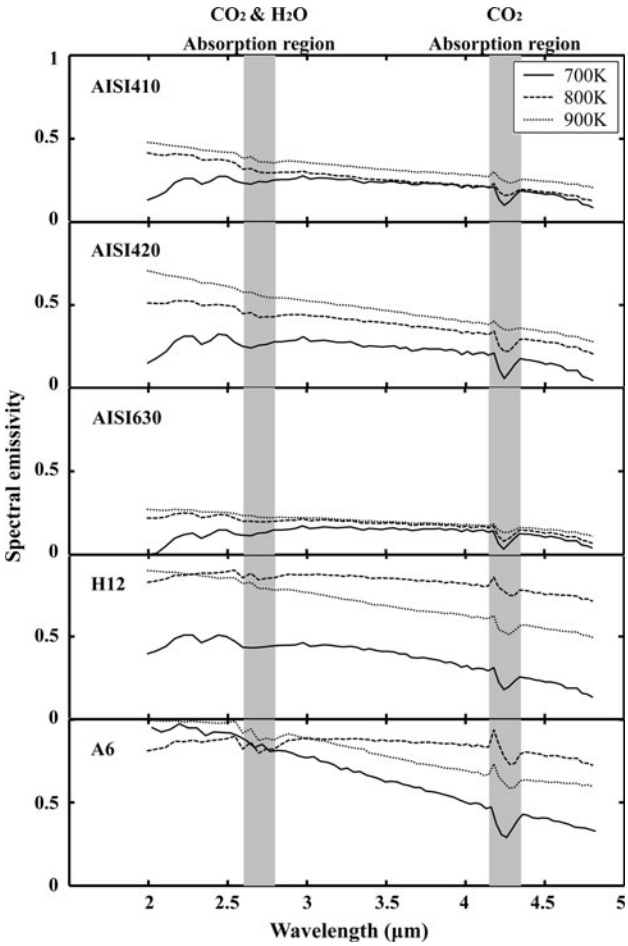

Fig. 5 Effects of wavelength and temperature on steel spectral emissivity

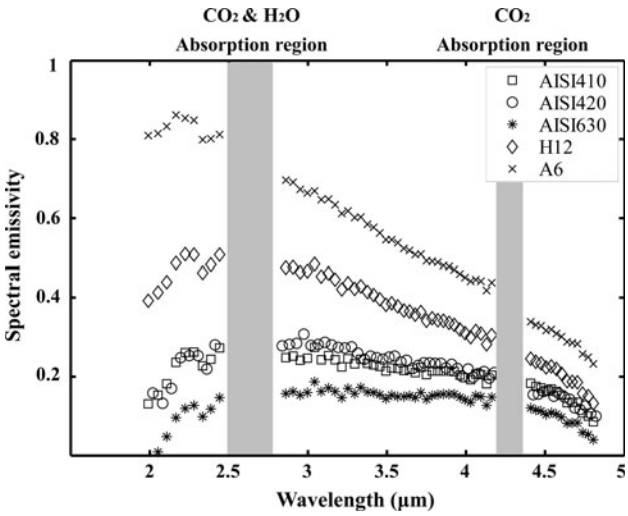

Fig. 6 Effects of alloy composition on spectral emissivity at 700 K

4.4 Effects of Heating Time

As shown in Fig. 7, tool steels, AISI A6 and AISI H12, with higher emissivity values have larger change in emissivity

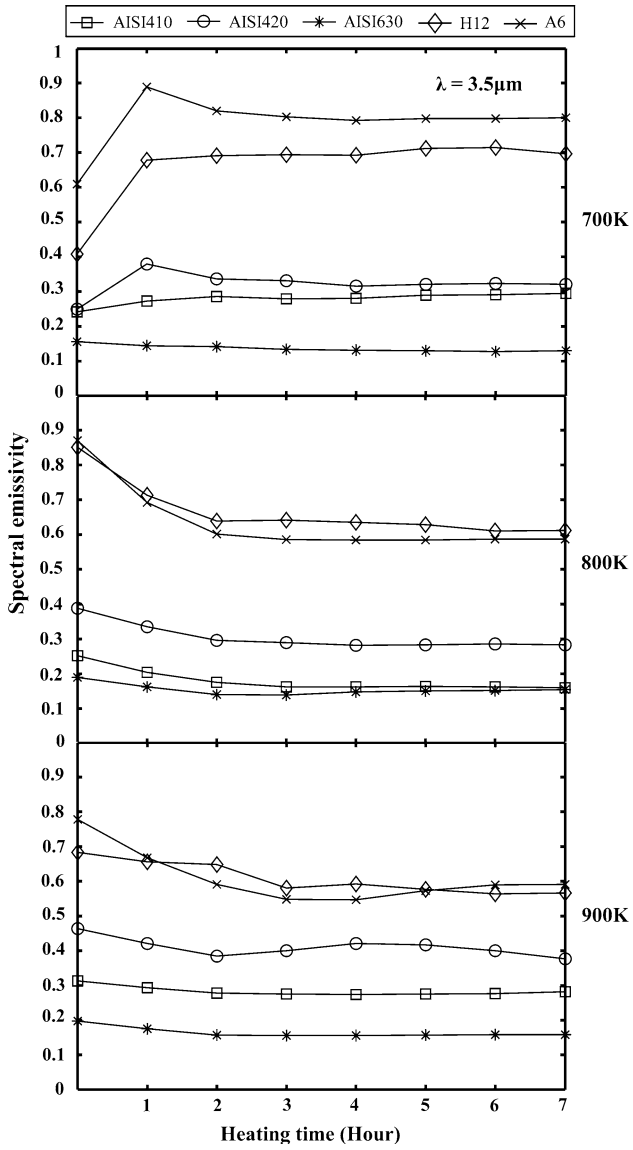

Fig. 7 Effects of heating time on spectral emissivity at 3.5 μm

during the initial 3-h heating. Only a slight change in emissivity is observed over the next 4 h for most alloys. The surface oxidation is known to contribute to the increase in emissivity value with the time-at-temperature heating. Therefore, the oxidation becomes fully developed after the initial 3-h heating.

5. Application of MRT Emissivity Models

Two most commonly used MRT emissivity compensation models are examined in this study. They are log-linear emissivity model (LLE) and linear emissivity model (LEM). Table 4 illustrates the percentage of inferred temperature error predicted by MRT using these two models in the spectral range from 2 to 4.8 μm. The CO_2 and H_2O bands shown in Fig. 5 are excluded from the examined wavelength range. Values exceeding 10% have been purposely deleted to help point out accurate models and their predictive trends. In Table 3, it includes results for two groups of steel samples: stainless steel (AISI 410, AISI 420, and AISI 630) and tool steel (AISI H12 and AISI A6), two different numbers of wavelengths (n and N), three different temperatures (700, 800, and 900 K), and polynomial functions up to third order with both models. The value n is the required minimum number of wavelength using least-squares technique, which is equal to the number of unknown coefficients in the emissivity model plus two, and N is the total number of wavelength available in the examined wavelength range. The third order is generally the upper limit in application of the LEM to adequately represent the complex emissivity behaviors of metallic surfaces.

A first look at the table appears to be somewhat puzzling. From the results, about half of the inferred temperature errors are under 10%. The occurrence of the accurate temperature predictions with errors under 1% is quite random: the first-order LLE model for AISI H12 and AISI A6 at 900 K have temperature errors from 0.3 to 0.9%; the second-order LLEs for AISI H12 at 900 K has temperature error of 0.6%; the first-order LEM for AISI A6 at 700 K has temperature error 0.3%, for AISI 420 at 800 K has temperature error 0.6%, and for AISI 630 at 900 K has temperature error 0.6%; the second-order LEM for AISI 410 and AISI 630 at 700 K have temperature errors from 0.14 to 0.3%, and for AISI H12 at 900 K, it has a temperature error of 0.1%.

Owing to the emissivity variations shown in Fig. 5, different orders of emissivity model are found suitable for different temperatures. At 700 K, the second-order and the third-order LEMs provide better temperature prediction because of the non-linear emissivity distributions of steel alloys from 2 to 4.8 μm. However, at 800 and 900 K, the emissivity spectrum becomes linear in the examined wavelength range, and the first-order LLE and the first-order LEM, therefore, come out with better results. Therefore, this shows that if the emissivity model can well represent the real emissivity behaviors, then the more accurate inferred temperature can be achieved.

One advantage of MRT is that the increase in the number of wavelengths allows MRT to statistically reduce the temperature errors due to measurement noise. However, as shown in Table 4, increasing the number of wavelengths does not significantly enhance measurement accuracy for most of the models. The required minimum number of wavelengths, n, actually gives satisfactory results. Therefore, it is sufficient to

Table 4 Percentage of temperature error in inferred temperature by MRT for steel samples at 700, 800 and 900 K

Inferred temperature errors, %, 2-4.8 μm												
Emissivity models:	**Log-linear emissivity model (LLE)**						**Linear emissivity model (LEM)**					
Order:	**First**		**Second**		**Third**		**First**		**Second**		**Third**	
Wave. No. (a):	***n***	***N***	***n***	***N***	***n***	***N***	***n***	***N***	***n***	***N***	***n***	***N***
True temperature												
700 K												
AISI 410									5	0.3	7.4	9.6
AISI 420									6.14	1.4	2.1	9.9
AISI 630									0.14	0.3		8.3
H12				3			8.6	7.7	8.85	5.6	1.7	0.9
A6							1.9	0.3		3.7		
800 K												
AISI 410	1.8	5.1	6.02				6.3	3.9	8			
AISI 420	5.4						0.6	7		8.9	6	9.5
AISI 630							9.9	6.1		9		
H12	5.1	2.3	6.4	6.6			5.5	1.1	7.75			9.1
A6	7.3	9.1	9.1	8.6			6.5	7.9	5.57	4.9		
900 K												
AISI 410	5.4	2.4	9.7				7.1	6.4				
AISI 420	5.9		8.1	5.6			8.9			4.1		
AISI 630	3.4	4.2					0.6	2.4				
H12	0.3	0.9		0.6			1.7	2		0.1		
A6	1	0.6					1.6	1.8		7.8	4.9	4.4

Missing values correspond to errors beyond 10%

(a) Wave. No. represents the number of wavelength: n is minimum number of wavelength required in MRT model and N is total number of wavelength available in the examined wavelength range

Table 5 The best model and the percentage of temperature error for each steel sample

Sample	Best emissivity model (percentage of temperature error)					
Temperature:	700 K		800 K		900 K	
Wave. No. (a):	*n*	*N*	*n*	*N*	*n*	*N*
AISI 410	2nd LEM (5)	2nd LEM (0.3)	1st LLE (1.8)	1st LEM (3.9)	1st LLE (5.4)	1st LLE (2.4)
AISI 420	3rd LEM (2.1)	2nd LEM (1.4)	1st LEM (0.6)	1st LEM (7)	1st LLE (5.9)	2nd LEM (4.1)
AISI 630	2nd LEM (0.1)	2nd LEM (0.3)	1st LEM (9.9)	1st LEM (6.1)	1st LEM (0.6)	1st LEM (2.4)
H12	3rd LEM (1.7)	3rd LEM (0.9)	1st LLE (5.1)	1st LEM (1.1)	1st LLE (0.3)	2nd LEM (0.1)
A6	1st LEM (1.9)	1st LEM (0.3)	2nd LEM (5.6)	2nd LEM (4.9)	1st LLE (1)	1st LLE (0.6)

(a) Wave. No. represents the number of wavelength: *n* is minimum number of wavelength required in MRT model and *N* is total number of wavelength available in the examined wavelength range

employ the required minimum number of wavelengths to infer the temperature and save the time on computation. This is consistent with earlier findings by Gathers (Ref 6), Doloresco (Ref 8), and Gardner et al. (Ref 10).

Statistically, LEM shows higher accuracy than LLE. Two emissivity models, the first-order LLE and the first-order LEM overall give good results on most occasions and provide the best compensation for different alloys, number of wavelengths, and temperatures. The third-order LLE shows the poorest compensation and is not recommended for steel samples in MRT.

The various percentages of inferred temperature error predicted by the best model for each alloy at different temperatures and number of wavelengths are shown in Table 5. Statistics show that the first-order and the second-order LEM occupy the most, and the first-order LLE come in second. Most of the best results of the second-order LEMs appear at 700 K because of nonlinear emissivity distribution explained earlier. The first-order LLE and the first-order LEM, not only achieve good temperature predictions for different alloys, the number of wavelengths, and temperatures, but also provide the smallest inferred temperature errors.

6. Conclusions

In this study, experiments were performed to measure the emissivity values for various steel samples. The effects of different parameters on spectral emissivity, such as wavelength, temperature, alloy composition, and heating time are investigated. Then, the experimental work is complemented by two commonly used MRT emissivity models, LLE and LEM, to predict the surface temperature. The application of the MRT emissivity models to steel alloys is examined and analyzed. Key findings from this study are discussed below:

(1) Overall, the spectral emissivity decreases with increasing wavelength and increases with increasing temperature.
(2) Steel with higher chromium content has lower emissivity value because of the chromium oxide protection layer.
(3) The spectral emissivity reaches steady state after the third-hour heating due to the surface oxidation becoming fully developed.
(4) Increasing the order of polynomial and increasing the number of wavelengths do not improve temperature measurement accuracy.
(5) The better the emissivity model with ability to suitably represent the real surface emissivity behaviors, the more accurate the inferred temperature by MRT.
(6) Overall, the first-order LEM and the first-order LLE give good results on most occasions and provide the best compensation for different alloys, the number of wavelengths, and temperatures.

Acknowledgments

The author is grateful for the support of the National Science Council of Taiwan (with project number NSC-94-2218-E-006-046). The author would also like to thank the Gloria Material Technology Corporation (GMTC) in Taiwan for the supply of steel samples, and Dr. Jongmook Lim of the Spectraline Inc. for the technical assistance and the instrument support.

References

1. M.A. Khan, C.D. Allemand, and T.W. Eager, Noncontact Temperature Measurement. II. Interpolation Based Techniques, *Rev. Sci. Instrum.*, 1991, **62**(2), p 403–409
2. Th. Duvaut, D. Georgeault, and J.L. Beaudoin, Multiwavelength Infrared Pyrometry: Optimization and Computer Simulations, *Infrared Phys. Technol.*, 1995, **36**, p 1089–1090
3. M. Hoch, The Integral Six-Color Pyrometer: A New General Method of Temperature Determination, *High Temp.-High Press.*, 1992, **24**, p 607–623
4. M. Hoch, The Integral Six-Color Pyrometer: Linear Dependence of the Radiance Temperature Tr on the Wavelength Lambda, *Rev. Sci. Instrum.,* 1992, **63**(4), p 2274–2281
5. G.R. Gathers, Monte Carlo Studies of Multiwavelength Pyrometry Using Linearized Equations, *Int. J. Thermophys.*, 1992, **13**(2), p 361–382
6. G.R. Gathers, Analysis of Multiwavelength Pyrometry Using Nonlinear Chi-Square Fits and Monte Carlo Methods, *Int. J. Thermophys.*, 1992, **13**(3), p 539–554
7. M.A. Pellerin, D.P. DeWitt, and G.J. Dail, Multispectral Radiation Thermometry for Aluminum Alloys, *Heat Transfer in Metals and Containerless Processing and Manufacturing*, Vol 162, T.L. Bergman, D.A. Zumbrunnen, Y. Bayazitoglu, and A.G. Lavine, Ed., ASME Heat Transfer Division, 1991, p 43–47
8. B.K. Doloresco, "Review of Multispectral Radiation Thermometry and Development of Constrained Minimization Method," M.S. Thesis, Purdue University, School of Mechanical Engineering, West Lafayette, IN, Dec 1986
9. M.F. Hopkins, *Four Color Pyrometer for Metal Emissivity Characterization*, Vol 2599, SPIE—The International Society of Optical Engineering, Philadelphia, PA, 1996, p 294–301

10. J.L. Gardner, T.P. Jones, and M.R. Davies, A Six-Wavelength Radiation Pyrometer, *High Temp.-High Press.*, 1981, **13**, p 459–466
11. J.L. Gardner, Computer Modeling of Multiwavelength Pyrometer for Measuring True Surface Temperature, *High Temp.-High Press.*, 1980, **12**, p 699–705
12. G.B. Hunter, C.D. Allemand, and T.W. Eager, Prototype Device for Multiwavelength Pyrometer, *Opt. Eng.*, 1986, **25**(11), p 1222–1231
13. M.A. Khan, C.D. Allemand, and T.W. Eager, Noncontact Temperature Measurement. I. Interpolation Based Techniques, *Rev. Sci. Instrum.*, 1991, **62**(2), p 392–402
14. M.A. Khan, ''Non-Contact Temperature Measurement,'' Ph.D. Thesis, Massachusetts Institute of Technology, Materials Engineering, Cambridge, MA, 1988
15. M. Battuello, T. Ricolfi, and L. Wang, Use of a Photodiode-array Spectroscopic System for Temperature Measurement, *Proc. of TEMPMEKO '93: 5th Int. Symp. on Temperature and Temperature Measurement in Industry and Science*, Prague, Czech Republic, 1993, p 150–155
16. J. Ji., J.P. Gore, Y.R. Sivathanu, and J. Lim, Fast Infrared Array Spectrometer Used for Radiation Measurements of Lean Premixed Flames, *Proc. of NHTC'00, 34th National Heat Transfer Conference*, 2000, Pittsburgh, PA, p 1–6
17. M.A. Pellerin, ''Multispectral Radiation Thermometry for Industrial Application,'' Ph.D. thesis, Purdue University, West Lafayette, IN, 1999
18. A. Otsuka, K. Hosono, R. Tanaka, K. Kitagawa, and N. Arai, A Survey of Hemispherical Total Emissivity of the Refractory Metals in Practical Use, *Energy*, 2005, **30**, p 535–543
19. G.R. Smolik, K.A. McCarthy, W.J. Garmack, and K. Coate, Mobilization from Austenitic Stainless Steel in Air and Steam: Recent Test, Compilation of Data from Tests to Data, and Resulting Dose Calculations, *Fusion Eng.*, *17th IEEE/NPSS Symposium*, Vol 1, 1997, p 161–166